

Fusing Landsat and MODIS Data for Vegetation Monitoring



IMAGE LICENSED BY INGRAM PUBLISHING

FENG GAO

USDA-ARS, Hydrology and Remote Sensing Laboratory,
Beltsville, MD 20705, USA
(e-mail: feng.gao@ars.usda.gov)

THOMAS HILKER

College of Forestry, Oregon State University,
Corvallis, OR 97331, USA
(e-mail: Thomas.Hilker@oregonstate.edu)

XIAOLIN ZHU

Department of Ecosystem Science and Sustainability,
Colorado State University, Fort Collins, CO 80523, USA
(e-mail: zhuxiaolin55@gmail.com)

MARTHA C. ANDERSON

USDA-ARS, Hydrology and Remote Sensing Laboratory,
Beltsville, MD 20705, USA
(e-mail: martha.anderson@ars.usda.gov)

JEFFREY G. MASEK

Biospheric Sciences Laboratory, NASA,
Goddard Space Flight Center, Greenbelt, MD 20771, USA
(e-mail: jeffrey.g.masek@nasa.gov)

PEIJUAN WANG

Institute of Eco-environment and Agro-meteorology,
Chinese Academy of Meteorological Sciences,
Beijing 100081, China
(e-mail: wangpj@cams.cma.gov.cn)

YUN YANG

USDA-ARS, Hydrology and Remote Sensing Laboratory,
Beltsville, MD 20705, USA
(e-mail: yun.yang@ars.usda.gov)

This work was supported in part by the NASA EOS program and the US Geological Survey (USGS) Landsat Science Team program. USDA is an equal opportunity provider and employer.

Abstract—Crop condition and natural vegetation monitoring require high resolution remote sensing imagery in both time and space – a requirement that cannot currently be satisfied by any single Earth observing sensor in isolation. The suite of available remote sensing instruments varies widely in terms of sensor characteristics, spatial resolution and acquisition frequency. For example, the Moderate-resolution Imaging Spectroradiometer (MODIS) provides daily global observations at 250m to 1km spatial resolution. While imagery from coarse resolution sensors such as MODIS are typically superior to finer resolution data in terms of their revisit frequency, they lack spatial detail to capture surface features for many applications. The Landsat satellite series provides medium spatial resolution (30m) imagery which is well suited to capturing surface details, but a long revisit cycle (16-day) has limited its use in describing daily surface changes. Data fusion approaches provide an alternative way to utilize observations from multiple sensors so that the fused results can provide higher value than can an individual sensor alone. In this paper, we review the Spatial and Temporal Adaptive Reflectance Fusion Model (STARFM) and two extended data fusion models (STAARCH and ESTARFM) that have been used to fuse MODIS and Landsat data. The fused MODIS-Landsat results inherit the spatial details of Landsat (30 m) and the temporal revisit frequency of MODIS (daily). The theoretical basis of the fusion approach is described and recent applications are presented. While these approaches can produce imagery with high spatiotemporal resolution, they still rely on the availability of actual satellite images and the quality of ingested remote sensing products. As a result, data fusion is useful for bridging gaps between medium resolution image acquisitions, but cannot replace actual satellite missions.

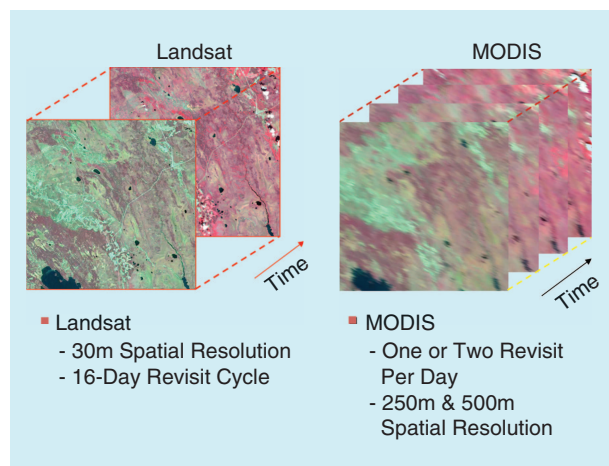


FIGURE 1. Landsat and MODIS data have complementary characteristics in terms of spatial and temporal resolution. Although they have been widely used for vegetation mapping and ecological monitoring, they may not be sufficient for applications that require high resolution imagery in both space and time.

I. INTRODUCTION

Climate change and human activities are having a remarkable impact on the Earth's land cover and land cover dynamics. Quantification of the type, magnitude, and the spatial distribution of these changes is important for climate mitigation and decision making processes [1], [2]. Satellite-based remote sensing provides valuable geospatial data for characterizing land cover and land cover dynamics at the globe scale. However, tradeoffs between spatial and temporal resolution result in satellite sensor designs that may be suboptimal for certain applications. For instance, moderate resolution sensors (a few hundred meters resolution or coarser) such as the Moderate-resolution Imaging Spectroradiometer (MODIS) sensors aboard the NASA EOS Terra and Aqua satellites can provide daily global observations that are valuable for capturing rapid surface changes at coarse spatial resolution. But the MODIS spatial resolution of 250–1000m is often inadequate for highly heterogeneous areas like agricultural landscapes. In contrast, Landsat data provide sufficient spatial detail (30m, here referred to as a medium spatial resolution) for monitoring land surface condition and change, particularly at scales of human activity [3]–[5]. But the 16-day revisit cycle and the presence of clouds have limited its use for studying global biophysical processes, which can evolve rapidly during the growing season. Fig. 1 illustrates the temporal and spatial characteristics of the Landsat and MODIS instruments. Remote sensing data with daily frequency and medium spatial resolution from a single sensor are not available today, largely as a result of prohibitive costs of such a system.

One way to construct daily observations at high spatial resolution is to combine remote sensing data from multiple sources. In order to fully use the complementary characteristics of different sensors, data fusion approaches have been developed to combine the spatial resolution of Landsat with the temporal frequency of coarse resolution MODIS. Traditional data fusion approaches were more focused on color blending or sharpening for visual enhancement. These approaches are also known as downscaling or sharpening techniques. Many image sharpening approaches use data from the same satellite platform or images from the same day. For example, the pan-sharpening technique uses a fine resolution panchromatic band to sharpen multi-spectral bands acquired at a coarser resolution by same instrument. Other traditional image fusion approaches include intensity-hue-saturation (IHS) modulation, as well as principal component analysis (PCA) and wavelet transformation, which can be treated as variants of the IHS technique [6]. In IHS, a multi-spectral image is converted from red, green and blue (RGB) space into the IHS space using a defined conversion matrix. The intensity image is then replaced by the finer resolution panchromatic band image and converted back to the RGB space using an inverse matrix. The resulting RGB image contains the spectral information (color) and the spatial details from panchromatic band. This approach is more focused on the image sharpness and better visualization; however,

it may cause color distortion due to the change of saturation [6]. Color distortion in the fused image breaks the law of energy conservation, which is critical for many quantitative remote sensing applications. Since these traditional data fusion methods have been well documented in the existing literature, we will not discuss them further in this paper.

Here, we are trying to solve a more complex problem – combining remote sensing data acquired from different sensors on different dates at very different spatial resolutions. The applications supported by these methods require data to be consistent (e.g., minimum color distortion). To accomplish this, physical parameters such as surface reflectance are used to develop the data fusion algorithm. The biophysical parameter provides a comparable measure from different sensors, i.e., the parameter acquired from fine resolution sensor can be aggregated and linearly related to coarse resolution sensor data when they are acquired from the same date and location. This is the basic requirement for our data fusion algorithms.

In the mid 2000s, a surface reflectance based data fusion approach - the Spatial and Temporal Adaptive Reflectance Fusion Model (STARFM) - was developed by Gao et al. [7]. STARFM uses comparisons of one or more pairs of observed Landsat and MODIS maps, collected on the same day, to predict maps at Landsat-scale on other MODIS observation dates. STARFM has been subsequently modified and extended for different applications to form the Spatial Temporal Adaptive Algorithm for mapping Reflectance Change (STAARCH) for detecting reflectance changes associated with land cover change and disturbance [8], and an enhanced STARFM (ESTARFM) developed to better handle more heterogeneous areas [9].

In this paper, we first describe Landsat and MODIS data characteristics, and then introduce the STARFM, STAARCH and ESTARFM data fusion methodologies. We then describe applications for data fusion in eco-physiological monitoring of vegetation development and water use.

II. LANDSAT AND MODIS DATA

The Landsat satellite series has provided a continuous Earth observation data record since the early 1970s. Landsats 1–3 carried the Multispectral Scanner System (MSS) instrument (with $68\text{m} \times 83\text{m}$ pixel resolution, resampled to 60m). In addition to MSS, Landsat 4 and 5 also carried the Thematic Mapper (TM) instrument, ushering in the age of the Landsat 30m pixel resolution. Landsat 5 was launched on March 1, 1984 and functioned for over 28 years until 2012. Landsat 7 was launched on April 15, 1999 and carries the Enhanced Thematic Mapper Plus (ETM+), which replicates the favorable 30m spatial resolution with improved accuracy in radiometric and geometric calibration. Both Landsat 5 and Landsat 7 include a thermal infrared band at a spatial resolution of 120m and 60m respectively. Landsat 8 was launched on February 11, 2013. The Landsat 8 satellite payload includes the Operational Land Imager (OLI) and the Thermal Infrared Sensor (TIRS). The OLI instrument provides 30 m resolution shortwave data, while TIRS collects and 100 m

resolution thermal infrared data on a 16 day repeat cycle. Landsat 5, 7 and 8 data during the MODIS era (after 2000) can be fused with the daily MODIS observations. Unfortunately, Landsat 7 ETM+ has suffered from the failure of the scan line corrector (SLC) since May 2003, causing image gaps (widening toward the Landsat scene edges) in the SLC-off mode. In early 2009, the U.S. Geological Survey (USGS) made all Landsat data freely available to the public, which led to a dramatic increase of data downloads and uses [4].

The Landsat data are routinely corrected radiometrically and geometrically (Level 1G) by the USGS Earth Resources Observation and Science (EROS) Center. Terrain correction (Level 1T) is applied using a Digital Elevation Model (DEM) and ground control points. USGS distributes shortwave Landsat data digital number (DN) and surface reflectance. They can be downloaded through the USGS Global Visualization Viewer (<http://glovis.usgs.gov/>) or the Earth Explorer (<http://earthexplorer.usgs.gov/>) website. The surface reflectance product is atmospherically corrected and is the basis for many high-level biophysical data products and for quantitative applications. The Landsat Ecosystem Disturbance Adaptive Processing System (LEDAPS) uses the MODIS 6S approach for atmospheric correction of Landsat TM, ETM+ and OLI shortwave data. The aerosol thickness is derived from the imagery itself at a coarse resolution [3], [10]. LEDAPS was first developed at NASA Goddard Space Flight Center (GSFC) for mapping forest disturbance and was later adopted and modified to produce the Landsat surface reflectance product at the USGS EROS center. The consistent surface reflectance products from the Landsat sensors provide a reliable medium resolution data source for data fusion.

MODIS is a key sensor aboard the NASA EOS Terra and Aqua satellites. Terra was launched on December 18, 1999. It orbits the Earth from north to south and passes the equator in the morning at around 10:30am. The Aqua satellite was launched on May 4, 2002. It orbits the Earth from south to north and passes the equator in the afternoon at around 1:30pm. As a result, MODIS on Terra and Aqua provide morning and afternoon observations for the entire Earth surface every one to two days. Since the MODIS sensor has a large swath width (2330 km), observations are available with even higher frequency at high latitudes. MODIS has 36 spectral bands covering the visible to thermal infrared wavelengths. Seven spectral bands were specifically designed for land applications with central band locations and bandwidths similar to Landsat TM/ETM+/OLI bands. Table 1 lists the bandwidths for TM, ETM+, OLI and MODIS. Spatial resolutions for MODIS bands vary from 250m to 1km . The TM and ETM+ bandwidths are wider than MODIS bands, especially for the near infrared band. Bandwidths for the Landsat 8 OLI are more similar to those on MODIS.

MODIS data products have been available since early 2000 and have been rigorously validated and are widely used in many applications. These data products integrate extensive remote sensing experience accumulated over several decades. A decade after the launch of Terra and Aqua,

TABLE 1. LANDSAT 5 TM, LANDSAT 7 ETM+, LANDSAT 8 OLI AND MODIS SENSOR CHARACTERISTICS.

LANDSAT 5 TM BANDWIDTH (μm)	LANDSAT 7 ETM+ BANDWIDTH (μm)	LANDSAT 8 OLI BANDWIDTH (μm)	MODIS BANDWIDTH (μm)	MODIS RESOLUTION (m)
B1: 0.45–0.52	B1: 0.441–0.514	B2: 0.452–0.512	B3: 0.459–0.479	500
B2: 0.53–0.61	B2: 0.519–0.601	B3: 0.533–0.590	B4: 0.545–0.565	500
B3: 0.63–0.69	B3: 0.631–0.692	B4: 0.636–0.673	B1: 0.620–0.670	250
			B15: 0.743–0.753	1000
B4: 0.78–0.90	B4: 0.772–0.898	B5: 0.851–0.879	B2: 0.841–0.876	250
B5: 1.55–1.75	B5: 1.547–1.749	B6: 1.566–1.651	B6: 1.628–1.652	500
B6: 10.4–12.5 (120m)	B6: 10.31–12.36 (60m)	B10: 10.60–11.19	B31: 10.78–11.28	1000
B7: 2.08–2.35	B7: 2.064–2.345	B11: 11.50–12.51	B32: 11.77–12.27	1000
			B7: 2.105–2.155	500

the MODIS data products are still continuing to improve, with a new Collection 6 release scheduled in the near future. Comparisons between MODIS and TM/ETM+ surface reflectance from same day observations demonstrate a high level of consistency [11]; however, differences still exist in terms of geometric, spectral and radiometric sensor characteristics. First, images acquired by MODIS cover a wide swath area and therefore view angles may vary from –55 degrees (forward scattering direction) to 55 degrees (backward scattering direction). The view angles within a Landsat scene vary within ± 7.5 degrees; thus, Landsat is normally regarded as a nadir-view sensor. The difference in view angle between MODIS and Landsat causes variations in surface reflectance due to bidirectional reflectance effects, especially for Landsat 5 and Landsat 8 which have different nadir-view visiting schedules to Terra and Aqua MODIS. Even though Landsat 7 and Terra were designed to have the same repeat (nadir-view visiting) schedule and thus ETM+ and MODIS can acquire images both at nadir-view on the same day, differences in acquisition time (Landsat is about 15–30 minutes earlier than MODIS and so solar angles are different) may still lead to data inconsistency. Second, the geolocation accuracy for Landsat imagery is normally less than one Landsat pixel. Although MODIS geolocation accuracy (50m for 1 standard deviation) is very good in terms of the MODIS pixel resolution (250m), the mismatch between Landsat and MODIS imagery can easily span a few Landsat pixels. Last but not least, the data processing approaches are different for the different sensors. We will further discuss these limitations and solutions in section IV.D.

III. SURFACE REFLECTANCE-BASED DATA FUSION APPROACHES

A. STARFM

A basic assumption for the STARFM data fusion approach is that changes in surface reflectance between different

dates are consistent and comparable at various resolutions if the area of interest has homogeneous land cover. Prior to applying data fusion approach, Landsat and MODIS observations are required to be calibrated and atmospherically corrected to surface reflectance. Both Landsat and MODIS images are co-registered and resampled to the same image size and extent. Since the Landsat pixel is the fine resolution pixel in the data processing, each Landsat pixel is regarded as a “pure” pixel even though it could be very heterogeneous at sub-pixel scales. Many Landsat pixels make up a coarse resolution MODIS pixel. If Landsat pixels are similar (same surface type or spectrally similar) within a MODIS pixel, we treat this MODIS pixel as a pure and homogeneous coarse resolution pixel. In such homogeneous areas, each Landsat pixel should be comparable to MODIS. In this simple case, the relationship between Landsat and MODIS can be simply expressed as

$$L(x, y, t_k) = M(x, y, t_k) + \varepsilon_k \quad (1)$$

where (x, y) is a given pixel location for both Landsat (L) and MODIS (M) images, t_k is the acquisition date for both the MODIS and Landsat data, and ε_k represents the difference between observed MODIS and Landsat surface reflectance (caused by differing bandwidth and data processing etc.). Here we assume that the MODIS data have been resampled to the 30m resolution of the Landsat image.

The approach further assumes that ground cover type and system errors at pixel (x, y) have not changed between the observation date t_k and the prediction date t_p , where a Landsat scene is not available. The temporal changes of surface reflectance from Landsat should be equivalent to the temporal changes in the corresponding MODIS pixel between two dates. If the bias between Landsat and MODIS stays same for two dates ($\varepsilon_p = \varepsilon_k$), we have

$$L(x, y, t_p) = L(x, y, t_k) + (M(x, y, t_p) - M(x, y, t_k)) \quad (2)$$

However, this ideal situation cannot often be satisfied from MODIS and Landsat observations. In most cases, MODIS pixels are not homogeneous and may include mixed land cover types when seen from a Landsat pixel resolution. To consider such mixed pixels in the prediction, STARFM introduces additional information from neighboring pixels and uses spectrally similar pixels in the prediction. That is, the predicted surface reflectance for the central pixel at date t_p is computed with a weighting

function from spectrally similar neighboring pixels within a specified search window:

$$L\left(\frac{w}{2}, \frac{w}{2} t_p\right) = \sum_{k=1}^P \sum_{i=1}^N W_{ik} \times (L(x_i, y_i, t_k) + (M(x_i, y_i, t_p) - M(x_i, y_i, t_k))) \quad (3)$$

where w is the searching window size and $(w/2, w/2)$ is the central pixel of this moving window. To ensure that correct information from neighboring pixels is used, only spectrally similar (i.e., from the same spectral class) and cloud-free pixels from Landsat surface reflectance within the moving window are used to compute reflectance. N represents the total number of similar Landsat pixels in the moving window and i is the index. P represents the total number of pairs of observed MODIS and Landsat images. The weighting function W_{ik} determines how much each neighboring pixel i contributes to the estimated reflectance of the central pixel from image pair k . It is determined by three measures, based on 1) spectral difference between the MODIS and ETM+ data at a given location; 2) temporal difference between the input MODIS data ($M(x_i, y_i, t_k)$) and the MODIS data on the prediction date ($M(x_i, y_i, t_p)$); and 3) geographic distance between the central pixel and the candidate pixel. Closer pixels are more highly weighted. Pixels with smaller spectral and temporal differences also receive higher weight. Weights for all spectrally similar pixels are normalized (so the sum of weights equals one) before applying to Eq. (3). These measures ensure that pure and close neighbor pixels get higher weights in the prediction.

Once the current central pixel is predicted, the algorithm will move onto the next Landsat pixel and a new central pixel and searching window will be formed. The approach uses an overlapping moving window technique. The spectrally similar neighboring pixels are determined by the difference of the central pixel to the neighboring pixel in the Landsat image within the searching window. A threshold of difference is pre-determined based on the statistics of the Landsat image. When the difference is less than the threshold, the neighboring pixel will be regarded as a spectrally similar pixel. As the approach does prediction band by band, the selection of spectrally similar pixels may be different for different bands. This process is different from land cover classification. For example, if two different surface types in one band show similar spectral reflectances, they will be treated as spectrally similar pixels for this band, but may be excluded if they are different enough (exceeding the threshold) in another band. The overlapped moving window technique ensures that the most spectrally similar pixels are selected for the best interest of the central (prediction) pixel. The procedure can be regarded as a dynamic classification process.

The STARFM approach has been tested using both simulated data and real satellite observations [7]. Validations were conducted by comparing the predicted MODIS-Landsat

surface reflectance to the actual Landsat surface reflectance on Landsat acquisition dates. Fig. 2 shows STARFM prediction results in the Boreal Forest, Canada. Two pairs of Landsat and MODIS images were acquired from May 24, 2001 and July 11, 2001 (the observation dates). Two additional MODIS images were acquired on June 4 and July 4, 2001 (the prediction dates). The STARFM algorithm was used to predict MODIS-Landsat surface reflectance on June 4 and July 4 using two image pairs on the observation dates and the MODIS images from the prediction dates. The predicted MODIS-Landsat images capture seasonal variations and also show spatial details that can only be observed at Landsat spatial resolution. STARFM can reasonably preserve the high spatial resolution of Landsat and high temporal resolution of MODIS if pure coarse resolution neighbor pixels can be found within the moving window. For complex mixtures of different land-cover types, performance degrades somewhat and adjustment of algorithm parameters (e.g., an increase in the moving window size) may be needed to improve prediction. STARFM can predict MODIS-Landsat images using one or two image pairs depending on available Landsat data, thus making it more flexible when clear Landsat images are hard to obtain in cloudy regions.

B. STAARCH

In STARFM, seasonal variability of vegetation is modeled using a temporal weight factor that assigns the highest weight to the temporally nearest satellite measurement. This technique has proven useful for detecting gradual changes in vegetation cover, but is less optimized for mapping sudden changes and disturbances, for instance as a result of human activities or fire. This is because in

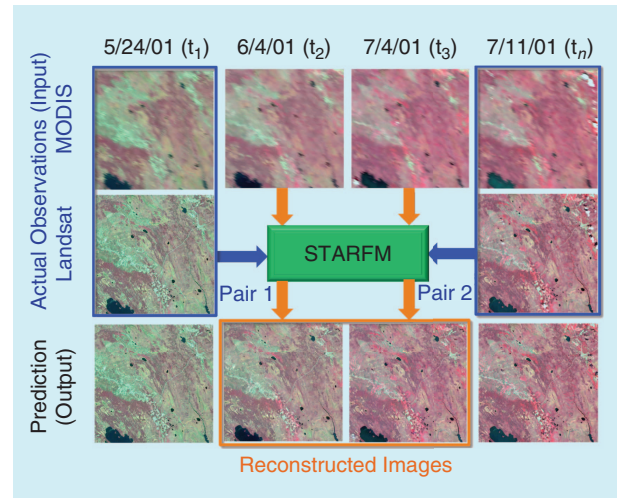


FIGURE 2. Predicted Landsat surface reflectance (bottom row) from daily MODIS reflectance imagery (top row) and Landsat/MODIS image pairs (in blue rectangles) over the BOREAS Southern Study Area, Canada (54°N, 104°W). In this example, Landsat observations are not available on 6/4 (t2) and 7/4 (t3) in 2001 (modified from Gao et al., 2006).

STARFM, the spatial structure of the landscape is obtained from Landsat images, regardless of whether these Landsat images were acquired before or after a change event. As an extension to the original algorithm, Hilker et al. [8] introduced the Spatial Temporal Adaptive Algorithm for mapping Reflectance Change (STAARCH). This algorithm is designed to detect changes in reflectance, denoting disturbance, using Tasseled Cap transformations of both Landsat TM/ETM+ and MODIS reflectance data. First, spatial delineation of disturbances is obtained from a change mask of a series of Landsat images based on Healey et al. [12]. Then, the date of disturbance (DoD) is identified for each disturbed pixel using a time series of all MODIS images collected in the interval between the two Landsat acquisitions, during which a disturbance occurred. Change detection in the MODIS time series is based on a MODIS version of the disturbance index (DI) [13] and the DoD is then defined as the date that saw the largest change in the series of this index (Fig. 3).

The output is a disturbance sequence in which all pixels that have been flagged as disturbed by the Landsat change mask are assigned the date at which the disturbance event most likely occurred. STAARCH also allows production of synthetic 30 m Landsat-like predictions of

surface reflectance, based on the STARFM algorithm [7]. However, STARFM generates Landsat-like images from a spatially weighted difference computed between a Landsat and a MODIS scene acquired on the observation date, and one or more MODIS scenes acquired at a prediction date [7]. In STAARCH, the base images consist of either the first or the last MODIS and Landsat pair in a given time series, depending upon which image pair best describes the land cover situation of a given pixel at the time of prediction. Two pairs of observed MODIS and Landsat are required for the prediction. The original implementation of STAARCH was based on eight-day composites of MODIS surface reflectance (MOD09A1/MYD09A1) [10]; however, other reflectance products could be used [8].

C. ESTARFM

STARFM can capture spatial details and vegetation phenology changes well for a homogeneous area. The accuracy, however, is degraded for a more heterogeneous and fragmented landscape [9], [14] where no pure MODIS pixels are available to provide accurate temporal changes of reflectance between two time points. The Enhanced STARFM (ESTARFM) approach was developed based on the STARFM method for improving the accuracy in heterogeneous landscapes [9].

Different from STARFM, which assumes that changes in Landsat pixels are equivalent to changes in the corresponding MODIS pixels, ESTARFM assumes that changes in Landsat pixels are *proportional* to the changes in the MODIS pixels. A conversion coefficient $v(x, y)$ is introduced to weight the change of the MODIS surface reflectance at the Landsat scale, modifying Eq. 2 as:

$$L(x, y, t_p) = L(x, y, t_k) + v(x, y) \times (M(x, y, t_p) - M(x, y, t_k)) \quad (4)$$

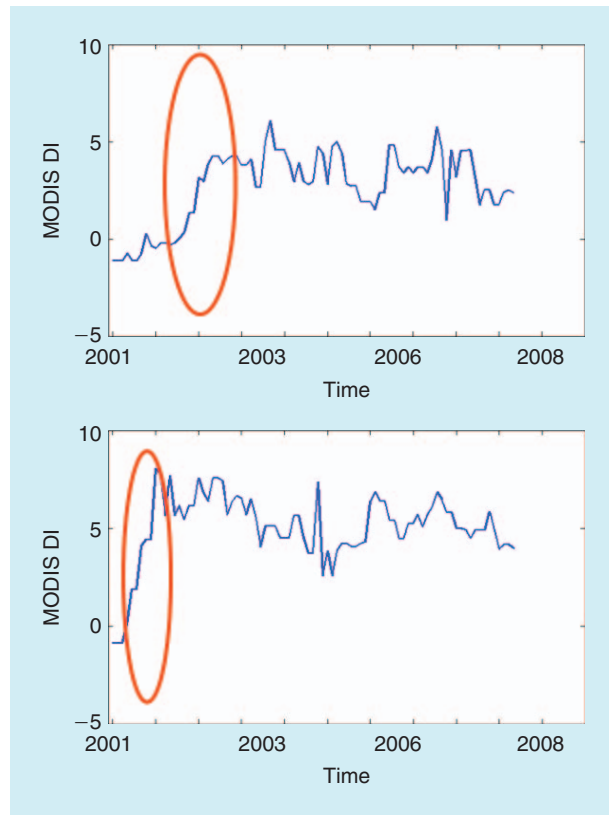


FIGURE 3. Example of a time series of MODIS-based disturbance indices for a relatively small stand-replacing disturbance event (~2.5ha in size) and a larger disturbance event that spans about 30ha in size. In both cases, the date of disturbance (DoD) can be determined from the “jump” in the disturbance index.

all Landsat pixels within a MODIS pixel that belong to same end-member class have same conversion coefficient, conversion coefficient of these same-class pixels can be estimated from the regression slope computed between their Landsat and MODIS reflectance values in two observed pairs. Similar to STARFM, ESTARFM also uses spectrally similar pixels within the moving window. The predicted reflectance for the central pixel at $(w/2, w/2)$ in the moving window based on two observed pair images can be computed as:

$$L\left(\frac{w}{2}, \frac{w}{2}, t_p\right) = \sum_{k=1}^2 T_k \times \left(L\left(\frac{w}{2}, \frac{w}{2}, t_k\right) \right. \\ \left. + \sum_{i=1}^N W_{ik} \times v(x_i, y_i) \times (M(x_i, y_i, t_p) - M(x_i, y_i, t_k)) \right) \quad (5)$$

where T_k determines the contribution from each pair of observed images. It is computed based on the change magnitude of MODIS images from prediction date to each of the two input pair dates at coarse resolution. The pair with smaller change magnitude contributes more to the final prediction in Eq. 5 assuming it gives a more accurate and reliable estimate.

D. COMPARISON OF THE STARFM, ESTARFM AND STAARCH FUSION APPROACHES

These three data fusion approaches – STARFM, ESTARFM and STAARCH - have been tested and applied in different studies published in the literature. They are all based on a common assumption - that temporal changes observed in near-daily MODIS imagery are indicative of changes that should be expected at Landsat scale, and therefore can create dense time-series of Landsat-like imagery. Biophysical variables such as surface reflectance are used to build a model that translates these changes between different sensors. All three approaches use spatial information from neighboring pixels to predict value for the central pixel. This is a fundamental difference from traditional data fusion approaches. It is a reasonable assumption that pixels having similar spectral properties or land cover type within a local area (moving window) will generally have a similar temporal change pattern. Despite these central core commonalities, the three data fusion approaches described here differ in terms of their specific application and limitations.

The ESTARFM approach considers the possibility of different change patterns for different land cover types within a heterogeneous MODIS pixel by introducing a landcover-related conversion coefficient. Comparisons between STARFM and ESTARFM in different sites have demonstrated the strengths of ESTARFM for producing Landsat-like images in more heterogeneous landscapes [9], [14]. Fig. 4 shows the observed Landsat ETM+ image (sub-area in Fig. 2) and the STARFM and ESTARFM fusion results using two pairs of Landsat and MODIS images. Both approaches capture temporal variations and

large land cover patches. The ESTARFM result shows clearer land cover boundaries than STARFM. Another comparison was conducted over a more heterogeneous area in central Virginia with smaller land cover patches. Fig. 5 shows the STARFM and ESTARFM fused images compared to the actual Landsat ETM+ image acquired on that same day (Feb. 26, 2002) over a more heterogeneous area. The ESTARFM result captured spatial details better than the original STARFM approach when two pairs of Landsat and MODIS image were used. However, the STARFM approach is more flexible and can use one input pair for prediction if it is properly selected. In Fig. 5, the

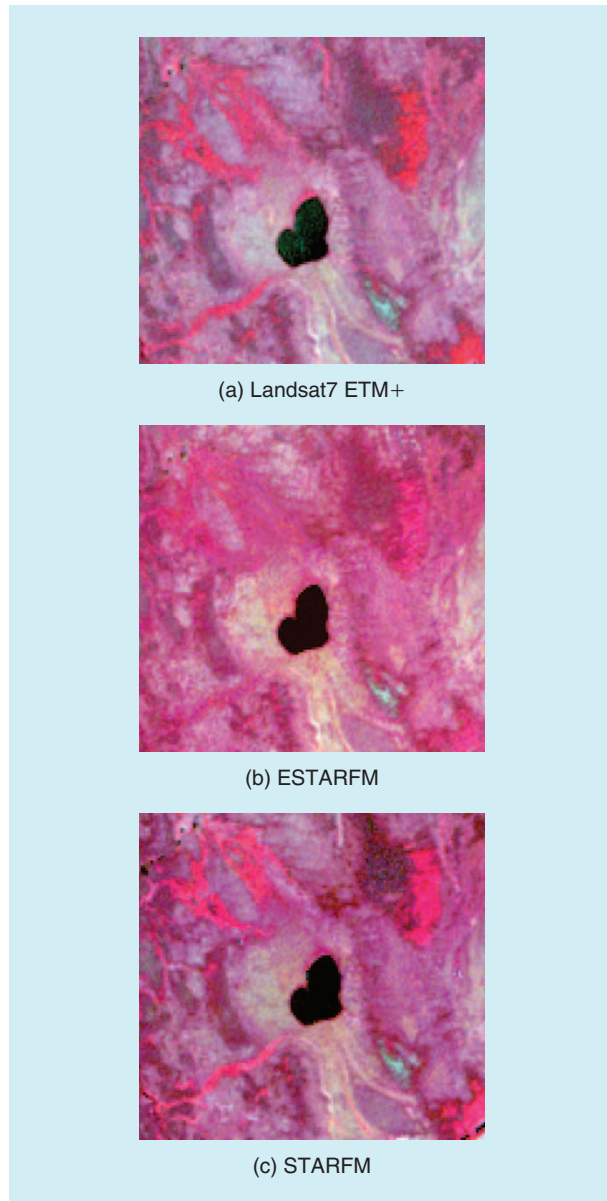


FIGURE 4. The observed Landsat 7 ETM+ (sub-area in Fig. 2) over the BOREAS Southern Study Area, Canada (54°N, 104°W) on July 11, 2011 (a) and data fusion results from ESTARFM (b) and STARFM (c) using image pairs from May 24 and August 12, 2011 (modified from Zhu et al., 2010).



FIGURE 5. Actual Landsat image over central Virginia (37°N , 77°W) acquired on 2/26/2002 (a) and the predictions of ESTARFM (b) and STARFM (c) using two pairs of images acquired on 1/25/2002 and 5/17/2012. The STARFM prediction using one input pair acquired on 1/25/2002 is shown in (d) (modified from Zhu et al., 2010).

STARFM result from one input pair (1/25/2002) shows similar result as ESTARFM in this example.

Nevertheless, the assumptions of ESTARFM may not valid in reality when a sudden change happen between the observation and prediction dates. In other words, the conversion coefficient estimated from the prediction period may not always constant during the period. In such case, the conversion coefficient in ESTARFM may introduce some uncertainties to the prediction than STARFM. Therefore, ESTARFM is not always superior to STARFM especially where the landscape is more homogenous and when temporal variance is dominant [14].

The STAARCH approach focuses on mapping forest disturbance using an appropriate MODIS-Landsat input pair collected before and after the time of disturbance event. Unlike STARFM, this approach can be applied to landscapes that have been abruptly changed during data fusion period. The prediction time period between two MODIS and Landsat pairs can be longer than for STARFM and ESTARFM. Limitations of the algorithm in its current form include the detection of disturbances smaller than two Landsat pixels, as the noise reduction algorithm implemented in the software will limit the size of disturbance features that can effectively be mapped to this resolution. Also, the STAARCH algorithm in its present form does not allow for the detection or progression of individual disturbance events. For instance, a cut block may have been established over a few weeks, with its size increasing over time.

In general, ESTARFM focuses on improving data fusion for the mixed pixels. The STAARCH approach focuses on detecting changes at Landsat-scale from the MODIS time-series and can improve data fusion over rapidly changing landscapes. Both ESTARFM and STAARCH require two MODIS and Landsat image pairs either to compute conversion coefficient or to develop the change mask required as input to the algorithms. The original STARFM approach can accept either one or two image pairs, making it more flexible in cloudy or data poor regions when Landsat imagery is scarce.

IV. ENVIRONMENTAL MONITORING APPLICATIONS FOR DATA FUSION

In recent years, the reflectance-based data fusion approaches described here have been successfully used in many different fields, such as generation of dense time-series of synthetic Landsat data for monitoring forest condition [15], [16], evaluating gross primary productivity [17], improving classification of conservation tillage [18], analyzing of dryland forest phenology [19], and mapping crop phenology at the field scales [20]. The approach has also been extended and applied for other biophysical parameters beyond reflectance, such as generating daily land surface temperature at Landsat pixel resolution for urban heat island studies [21] and mapping daily evapotranspiration (ET) at the field scales for crop water use monitoring [22], [23]. An operational STARFM framework has been implemented for routine monitoring of vegetation cover [24]. These studies show that data fusion can be effectively employed to capture both detailed spatial and temporal information about changing landsurface conditions.

A. FOREST MONITORING

Detailed information on forest ecosystems is important for a wide range of applications from ecological modeling [25] to estimating carbon budgets on regional and global scales. Forest disturbance in particular can fragment suitable habitat reducing forest patch size, result in loss of carbon stocks due to biomass burning or conversion of forests to agricultural lands [26], [27]. Between 2000 and 2012 alone, an estimated 2.3 million km² of forest was lost to deforestation or fire; in contrast, forest gain over the same time was only about 0.8 million km² [28]. The rapid nature and the scale of these changes poses challenges to the remote sensing community as comprehensive understanding of anthropogenic impacts and their feedbacks on ecosystems requires frequent [29] and comprehensive observations across large areas [30], [31], as statistically detectable change in vegetation depends on noise and sampling frequency. Global deforestation maps have only recently been implemented [28] at adequate spatial scales, but sufficient frequency is often still inhibited by cloud cover, particularly in tropical and boreal regions where most of the changes occur [28]. Data fusion approaches, such as the ones described in this paper, may help overcome some of these limitations by providing

frequent observation of forest cover, phenology and disturbance at 30m spatial resolution.

The predictability of changes in fine resolution synthetic images depends upon the capacity of MODIS to detect these changes, particularly when they occur in vegetation structure or stand composition or at sub-pixel ranges [7]. For instance, pixel brightness of fine resolution predictions can only be adjusted at coarse resolution scales. Consequently, our ability to identify change events is still limited by the extent to which MODIS data can be used to detect changes at sub-pixel range. Nonetheless, initial applications based on STARFM [15][18] and its derivatives such as STAARCH [8], [32] have demonstrated the improved ability of this approach to map changes in vegetation at landscape level scales. Most forestry based applications have been implemented in coniferous forest types, which are typical for large parts of western North America. Further research will need to investigate the potential of this technique, particularly in the tropical regions of this world, where changes are enormous but frequent cloud cover inhibits its timely

and accurate mapping with sufficient spatial and temporal detail.

B. CROP MONITORING

Crop progress and condition can be affected by climate changes, local weather, environment changes and human activities. Monitoring crop condition can help us to understand the impacts of these changes. Over the past three decades, both corn and soybean in the U.S. have been planted increasingly earlier in the spring. Corn planting dates have advanced by 10 days and soybean by 12 days from 1981 to 2005 [1]. This earlier planting has been accompanied by a longer growing season, both of which contribute to yield increases. In addition to the climate and weather changes, crop phenology trends also reflect changing farm management strategies and development of new cold- and drought-hardy genotypes [33]. High spatial and temporal resolution information is required to map the changes at field scales.

Using the STARFM data fusion approach, Gao et al. [20] built Landsat NDVI time-series at daily frequency for central Iowa. Fig. 6 shows the NDVI trends computed

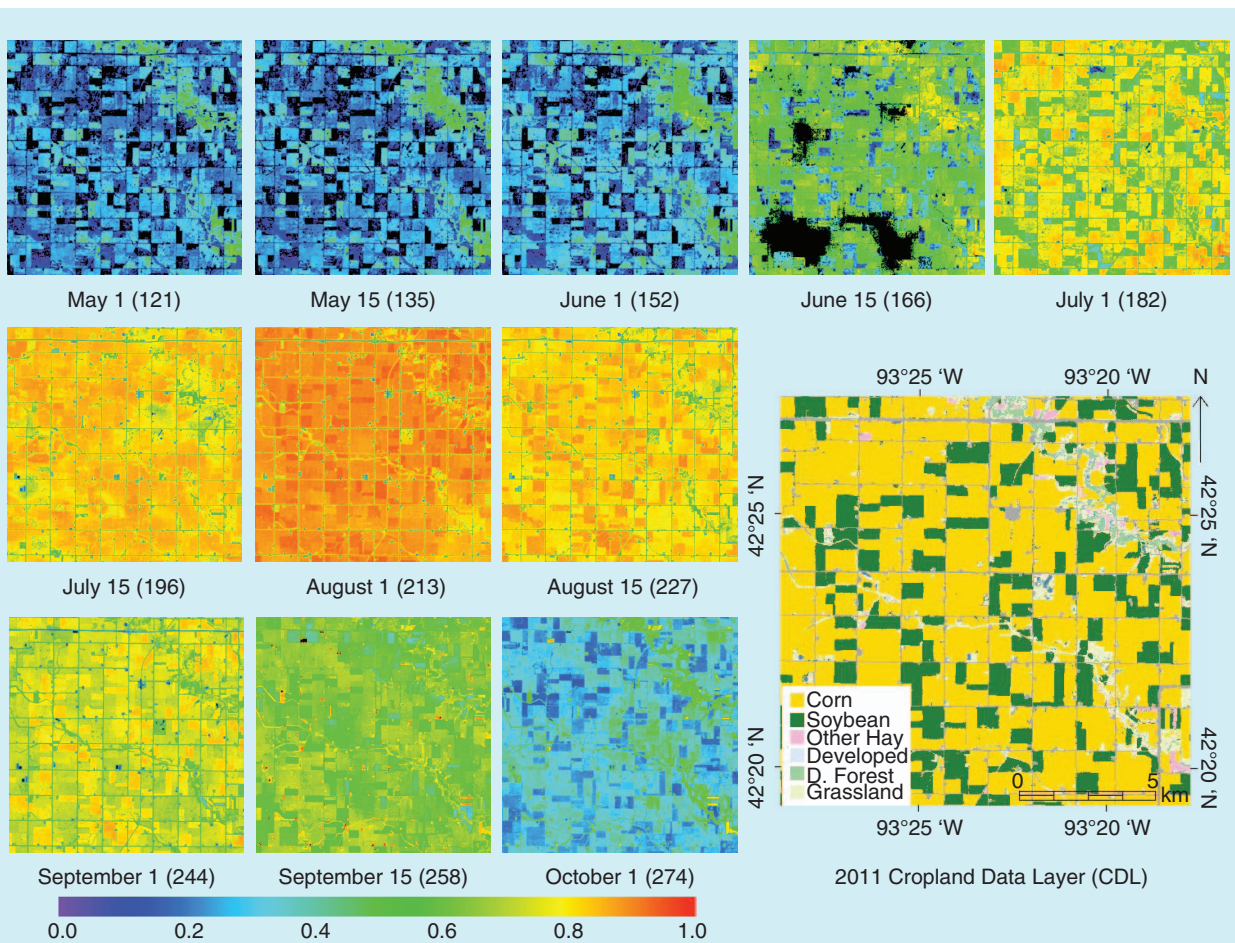


FIGURE 6. Daily Landsat NDVI (shown every half month) computed from MODIS-Landsat STARFM fusion of red and NIR band data from May 1 to October 1, 2011 over central Iowa. The Cropland Data Layer (CDL) for the same area for 2011 is shown in the lower right corner (modified from Gao et al., 2013).

from fused MODIS-Landsat reflectance time series in the red and NIR bands during the 2011 growing season in central Iowa (subset of Landsat path 26 and row 31). As shown in the 2011 cropland data layer (lower right image), this area is a rain-fed agricultural region and mostly planted corn and soybeans. Other natural vegetation types include deciduous forest and grasslands. The corn and soybean fields are normally rotated in consecutive years. Different temporal trends of NDVI can be observed for different surface types during the growing season. Deciduous forest (in northeast of the image) shows an earlier green-up, followed by corn and soybeans. Most of the crop fields show maximum NDVI around August 1. Crop NDVI values drop quickly in early October as the crops senesce.

These daily NDVI time-series were analyzed using the TIMESAT phenology program [34]. Crop phenological metrics such as the dates of the start of the season and end of the season were extracted and compared to crop progress reports collected by the USDA National Agricultural Statistics Service (NASS). USDA NASS collects crop progress and condition data reported at the county by trained observers. These individual reports are aggregated over a larger area (state or sub-state) before public release. High correlations were found between the NASS-reported soybean emergence date and the start of the season from TIMESAT. The end of the season date agrees with the reported harvest time [20]. By using the data fusion approach and connecting the remote sensing

detected phenology metrics to the crop growth stages, we will be able to map crop growth at field scales and provide useful information for monitoring crop conditions and forecasting yields.

C. DAILY FIELD-SCALE EVAPOTRANSPIRATION

Evapotranspiration (ET) describes the net exchange of water vapor between the Earth's surface and the atmosphere. Over land, ET is comprised primarily of water transpired by vegetation and water evaporated directly from the soil or leaf surfaces. Remotely sensed maps of ET can provide spatial and temporal information about how water is consumptively used over landscapes, and can be a valuable tool for managing freshwater resources at field to basin scales. In particular, land surface temperature retrieved from thermal infrared (TIR) satellite imagery has proven to be a useful diagnostic of surface moisture conditions and evaporative fluxes [35].

For agricultural water management, ET information is most beneficial at sub-field scales (~100 m resolution or finer) and daily timesteps [36]. Unfortunately, TIR imagery is not routinely available globally with this spatiotemporal frequency. A single fully functional Landsat provides images at 16-day intervals, or 8 days in the overlap regions. However, in regions of persistent cloudiness, we may be fortunate to acquire 2 or 3 clear scenes during a growing season. To improve temporal sampling in seasonal water use curves at Landsat scale, STARFM has been employed to fuse 1-km ET retrievals from MODIS TIR imagery at

approximately daily timesteps with periodic Landsat-based retrievals at 30-m resolution, using TIR imagery sharpened to the short-wave band resolution [7]. While STARFM was originally designed for fusing reflectance data, experiments have demonstrated utility for fusing ET data as well.

The ET fusion approach has been evaluated over several agricultural landscapes in comparison with ground-based measurements collected at micrometeorological flux tower sites in both irrigated and rainfed cropping systems [22], [23]. The greatest benefit of STARFM over a Landsat-only interpolation to daily timesteps has been observed when significant precipitation occurs between successive clear-sky Landsat overpasses, resulting in a discontinuous change in soil moisture and evaporative flux. Assuming the rainfall event is reasonably resolved at the 1-km scale, MODIS TIR is able to convey timely information regarding the change in moisture status (expressed by a depressed surface temperature signal) during the gap between Landsat overpasses (Fig. 7). Landsat, in turn, provides high spatial frequency structure to the resulting fused ET timeseries.

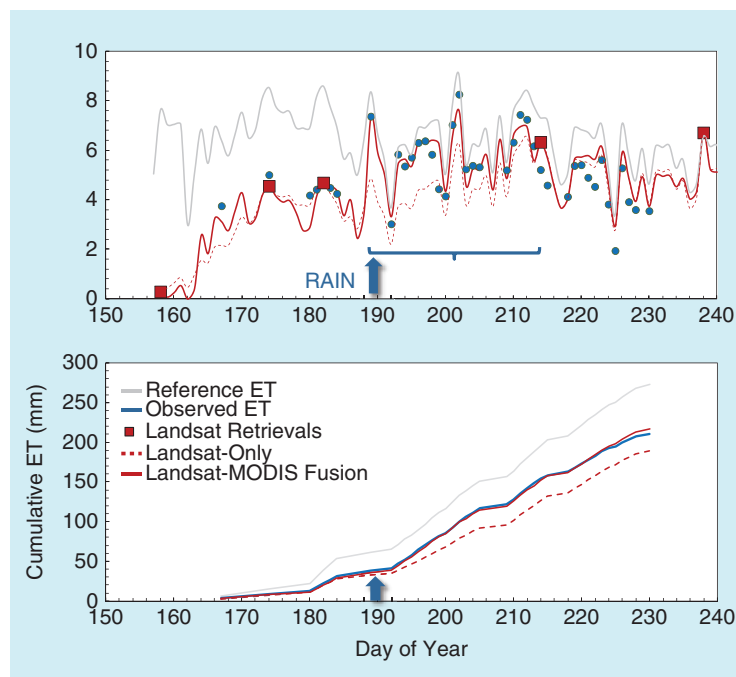


FIGURE 7. Daily (top) and cumulative (bottom) ET retrieved using Landsat-MODIS data fusion and with a Landsat-only interpolation compared to observed fluxes. The fused timeseries better captures ET response to the rainfall event around day of year 190.

Fig. 8 demonstrates an application of ET data fusion over a managed loblolly pine plantation in the coastal plains of North Carolina. Studies in this plantation have demonstrated a stand-age dependence of water use and drought response to drought - presumably related to tree rooting depth [37], [38]. Strong heterogeneity in a map of seasonal water use is observed over this managed forest system, accumulated from daily fused ET data at 30m resolution over the 2013 growing season, even using only a few clear-sky Landsat scenes. The fused results reasonable reproduce daily measurements of ET made in a 20-year old stand and a newly clearcut stand within the modeling scene. Multi-year high spatiotemporal resolution ET datacubes, developed using STARFM data fusion, can be effectively mined to investigate water use response to climate and management forcings.

D. OPERATIONAL STARFM FRAMEWORK

Data fusion approaches assume remote sensing data from different sensors are consistent and comparable. Even when Landsat and MODIS data have been carefully geo-registered, radiometrically calibrated and atmospherically corrected, they may be inconsistent for many reasons. In order to reduce these inconsistencies and make the data fusion system more robust, an operational STARFM data fusion framework has been built [24]. Compared to earlier implementations of STARFM, several improvements have been incorporated in this framework. These include viewing angle correction to the MODIS daily bidirectional reflectance, automated co-registration of MODIS and Landsat pair images, and automatic selection of Landsat and MODIS image pairs used as input to STARFM.

Data fusion tools can use MODIS daily surface reflectance or MODIS nadir-bidirectional reflectance distribution function (BRDF) adjusted reflectance (NBAR) to fuse with Landsat. The MODIS NBAR product is a 16-day product and may not agree with Landsat data on a specific day especially during period of rapid vegetation growth. The MODIS daily surface reflectance is a directional reflectance product which is affected by BRDF effects; i.e., the surface reflectance varies with viewing and illumination angles, whereas the Landsat TM, ETM+ and OLI instruments are normally regarded as nadir-viewing instruments. To minimize MODIS-Landsat differences due to viewing angle, the operational STARFM framework corrects the MODIS daily directional reflectance to nadir-viewing reflectance. A magnitude BRDF inversion

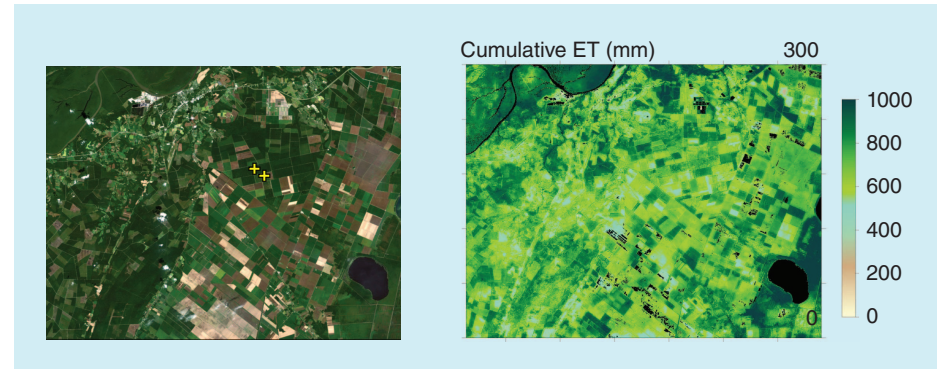


FIGURE 8. Cumulative ET from day of year 100 to 300 over a managed pine plantation in the North Carolina coastal plains (right). Yellow crosses in true-color Landsat image (left) indicate locations of flux towers in mature and clear-cut stands.

approach (backup algorithm for the MODIS BRDF/Albedo products [39]) is used to correct MODIS daily surface reflectance to daily NBAR data. BRDF parameters for each pixel are extracted from the MODIS BRDF parameters (MCD43A1) product. Since MODIS BRDF is a 16-day product with 8-day overlap, we select the 16-day period that best covers the Landsat acquisition date.

Landsat and MODIS images have different geolocation accuracy. Although the geolocation accuracy for MODIS is very good in term of MODIS pixel resolution, it may still in a few Landsat pixels. Since data fusion is performed at Landsat pixel resolution, a better co-registration between Landsat and MODIS is required. In the operational data fusion framework, we implemented the automatic image co-registration process by computing and searching the maximum correlation between Landsat and MODIS images. If the location of the maximum correlation is different from current location (directly reprojected using the MODIS reprojection tool), the MODIS image will be shifted to the Landsat location which produces the maximum correlation.

The operational framework allows selection of input pair images either automatically or manually. The manual option allows definition of pair images for any prediction date. The automatic option was implemented in two ways. One is to choose the pair image closest to the prediction date. The other option is to select the MODIS-Landsat pair image that has a higher correlation coefficient with MODIS images between two bracket pair dates.

The STARFM approach uses an overlapped searching window for each prediction. It can be very time consuming in searching for spectrally similar pixels. Recently, we implemented an improved algorithm that allows combining of multiple predictions together if the pair images are the same. When the same pair images are used, the searching process for spectrally similar pixels is the same and therefore we only need search once and then run predictions for many prediction dates. This implementation greatly improves computing efficiency when running data fusion for many dates. In our tests, it is 15 times faster for 30 predictions (same pair) using the improved algorithm comparing

the original program that requires to run 30 times individually. Since we do prediction pixel by pixel, it is also straightforward to enable parallel computing for a multi-processor system. These improvements allow applications of the data fusion approach over large areas. The recently improved STARFM software package can be downloaded from the USDA ARS software website.

Many of the improvements discussed here for the operational STARFM data fusion framework can also benefit other data fusion approaches as well.

V. DISCUSSION

Data fusion approaches have been applied to synthesize remote sensing imagery from multiple sources with different spatial, temporal and spectral characteristics, such that the fused result can convey more information than can an individual sensor alone. Traditional data fusion approaches such as the IHS-like methods aim to sharpen multi-spectral band imagery using panchromatic band imagery. That approach focuses on fusing spectral information with spatial features. The data fusion approaches presented in this paper aim to fuse images acquired from different sensors and dates at very different spatial resolutions. The main objective of this kind of data fusion is to generate dense time-series of remote sensing data at a finer spatial resolution and thus the focus is on fusing spatial and temporal features using same multi-spectral band imagery.

The currently existing body of literature has demonstrated the capability of STARFM, STAARCH and ESTARFM to monitor changes of terrestrial ecosystems with added benefit over using single sensor approaches. Most data fusion techniques, including the approaches and examples in this paper, are based on Landsat and MODIS data since they have similar spectral bands and more importantly they are freely and can be easily accessed to the public. However, the techniques described in this paper could equally be extended to other, similar sensors. For example, the Visible Infrared Imaging Radiometer Suite (VIIRS) on board the Suomi-National Polar-orbiting Partnership (NPP) mission (launched on October 28, 2011) and planned Joint Polar Satellite System (JPSS) missions provide visible to shortwave spectral bands at 375 and 750 m resolution, as well as TIR data. The VIIRS instrument inherits attributes from MODIS and AVHRR. Its configuration makes it an ideal high frequency data source for data fusion approaches. The recently launched Sentinel-2 mission from European Space Agency (ESA) provides additional multiple spectral band images at 10 to 20 m resolution. The Sentinel-2 data will be freely available and should be an ideal high spatial resolution data source for data fusion.

Even though the data fusion approach can be used to make synthetic images from multiple sources, these fused images cannot replace actual images from satellite missions especially when surface changes are rapid and subtle. Changes that are missed (e.g. due to clouds)

or not sensible (too small) in the coarse resolution images cannot be reconstructed. The data fusion models have limitations on predicting dates that are distant from the available image pairs. For instance, the predictability of changes in the fine resolution synthetic images depends on the capacity of at least one sensor to detect these changes in space and time, particularly when they occur in vegetation structure or stand composition or at sub-pixel ranges [7]. More actual medium resolution images can therefore help to capture small changes and to shorten prediction period and thus reduce uncertainties of data fusion results. By combining existing satellite observations and fused results we will be able to perform time-series analyses at medium spatial resolution and to investigate landscape changes at spatiotemporal resolutions that have been heretofore inaccessible.

AUTHOR INFORMATION



Feng Gao received the B.A. degree in geology and the M.E. degree in remote sensing from Zhejiang University, Hangzhou, China, in 1989 and 1992, respectively, the Ph.D. degree in geography from Beijing Normal University, Beijing, China, in 1998, and the M.S. degree in computer science from Boston University, Boston, MA, USA, in 2003. From 1992 to 1998, he was a Research Assistant at the Nanjing Institute of Geography and Limnology, Chinese Academy of Science, Nanjing, China. From 1998 to 2004, he was a Research Associate Professor at the Department of Geography and a Researcher in the Center for Remote Sensing, Boston University. From 2004 to 2011, he was a Research Scientist with Earth Resources Technology, Inc. and the NASA Goddard Space Flight Center. Since 2011, he has been a Research Scientist with the Hydrology and Remote Sensing Laboratory, USDA Agricultural Research Service. His recent research interests include remote sensing modeling, multi-sensor data fusion, and vegetation biophysical parameter retrieving for crop and ecosystem condition monitoring. He is currently a member of the Landsat Science Team and the MODIS Science Team.



Thomas Hilker obtained a PhD from the University of British Columbia (UBC), Canada, in 2008 and have worked at UBC (2008–2011) and NASA's Goddard Space Flight Center (2011–2012). Currently, he is holding a position as Assistant Professor at Oregon State University. His research interest is in remote sensing of terrestrial ecosystems, particularly the carbon, water and energy balance. Earth system science is currently at the crossroads as it is faced with the daunting task of assessing the risks of anthropogenic changes to Earth and atmosphere, their feedbacks on global ecosystems and consequences for life on earth. To meet these challenges, development and application of models and algorithms is needed for retrieving ecosystem states and fates from remote sensing data. His research philosophy and guiding principles

include efficient data handling and analysis, scientific rigor in its evaluation and effective communication of the results.



Xiaolin Zhu received the B.S. degree in Resource Science and Engineering and the M.S. degree in Civil Engineering from Beijing Normal University, China, in 2007 and 2010 respectively, and Ph.D. degree in Geography from The Ohio State University, Columbus, USA, in 2014. He is currently a postdoctoral researcher in the Department of Ecosystem Science and Sustainability, Colorado State University. His research interests include remote sensing image processing, data fusion, quantitative information retrieval, spatiotemporal analysis, and land surface dynamic monitoring.



Martha C. Anderson received a B.A. degree in Physics from Carleton College, Northfield, MN, in 1987, and a PhD in Astrophysics from the University of Minnesota, Minneapolis, in 1993. Presently she is a Research Physical Scientist for the USDA Agricultural Research Service in the Hydrology and Remote Sensing Laboratory in Beltsville, MD. Her research interests focus on mapping water, energy, and carbon land-surface fluxes at field to continental scales using thermal remote sensing, with applications in drought monitoring and soil moisture estimation. She is currently a member of the Landsat Science Team and HypSIRI Science Working Group.



Jeffrey G. Masek received the B.A. degree in geology from Haverford College, Haverford, PA, USA, in 1989 and the Ph.D. degree in geological sciences from Cornell University, Ithaca, NY, USA, in 1994. He is currently a Research Scientist with the Biospheric Sciences Laboratory, NASA Goddard Space Flight Center, Greenbelt, MD, USA. He also serves as the NASA Landsat Project Scientist, and has previously held positions at University of Maryland, College Park, MD, USA; Hughes Information Systems; and Cornell University. His research interests include mapping land cover change in temperate environments, application of advanced computing to remote sensing, and satellite remote sensing techniques.



Peijuan Wang received the B.A. degree in computer sciences from Inner Mongolia Normal University, Huhehot, China, in 2001, and the Ph.D. degree in geography and GIS from Beijing Normal University, Beijing, China, in 2006. From 2006 to 2008, she was a Research Assistant at Chinese Academy of Meteorological Sciences, China Meteorological Administration, Beijing, China. Since August 2008, she is a Research Associate Professor. Her research interests include agricultural remote sensing modeling and the effects of climate change on agriculture.



Yun Yang received the B.S. degree in geography from Beijing Normal University, Beijing, China, in 2004, the M.S. degree in Environmental Sciences from the University of Massachusetts, Boston, MA, USA, in 2012 and the Ph.D. degree in Environmental Sciences from the University of Massachusetts, Boston, MA, USA, in 2013. Since 2014, she has been a research physical scientist with the Hydrology and Remote Sensing Laboratory, USDA Agricultural Research Service. Her recent research interests include water and energy flux mapping at field scale using multisensor data fusion and drought monitoring and early detection using thermal remote sensing.

REFERENCES

- [1] C. J. Walther, J. Hatfield, P. Backlund, L. Lengnick, E. Marshall, M. Walsh, S. Adkins, M. Aillery, E. A. Ainsworth, C. Ammann, C. J. Anderson, I. Bartomeus, L. H. Baumgard, F. Booker, B. Bradley, D. M. Blumenthal, J. Bunce, K. Burkey, S. M. Dabney, and J. A. Delg, "Climate change and agriculture in the united states: Effects and adaptation," *USDA Technical Bulletin 1935*, Washington, D.C., Feb. 2012.
- [2] C. B. Field, V. Barros, T. F. Stocker, D. Qin, D. J. Dokken, K. L. Ebi, M. D. Mastrandrea, K. J. Mach, G.-K. Plattner, S. K. Allen, M. Tignor, and P. M. Midgley, Ed., *Intergovernmental Panel on Climate Change (IPCC), Managing the Risks of Extreme Events and Disasters to Advance Climate Change Adaptation*. Cambridge, U.K.: Cambridge Univ. Press, 2012, pp. 1–584.
- [3] G. Masek, E. F. Vermote, N. Saleous, R. Wolfe, F. G. Hall, F. Huemmrich, F. Gao, J. Kutler, and T. K. Lim, "A Landsat surface reflectance data set for North America, 1990–2000," *Geosci. Remote Sensing Lett.*, vol. 3, no. 1, pp. 68–72, Jan. 2006.
- [4] M. A. Wulder, J. G. Masek, W. B. Cohen, T. R. Loveland, and C. E. Woodcock, "Opening the archive: How free data has enabled the science and monitoring promise of Landsat," *Remote Sens. Environ.*, vol. 122, pp. 2–10, July 2012.
- [5] D. Roy, M. A. Wulder, T. R. Loveland, C. E. Woodcock, R. G. Allen, M. C. Anderson, D. Helder, J. R. Irons, D. M. Johnson, R. Kennedy, T. A. Scambos, C. B. Schaaf, J. R. Schott, Y. Sheng, E. F. Vermote, A. S. Belward, R. Bindschadler, W. B. Cohen, F. Gao, J. D. Hipple, P. Hostert, J. Huntington, C. O. Justice, A. Kilic, V. Kovalskyy, Z. P. Lee, L. Lymburner, J. G. Masek, J. McCormick, Y. Shuai, R. Trezza, J. Vogelmann, R. H. Wynne, and Z. Zhu, "Landsat-8: Science and product vision for terrestrial global change research," *Remote Sens. Environ.*, vol. 145, pp. 154–172, Apr. 2014.
- [6] T. Tu, S. Su, H. Shyu, and P. Huang, "A new look at HIS-like image fusion methods," *Inform. Fusion*, vol. 2, no. 3, pp. 177–186, Sept. 2001.
- [7] F. Gao, J. Masek, M. Schwaller, and F. Hall, "On the blending of the Landsat and MODIS surface reflectance: Predicting daily Landsat surface reflectance," *IEEE Trans. Geosci. Remote Sensing*, vol. 44, no. 8, pp. 2207–2218, Aug. 2006.
- [8] T. Hilker, A. M. Wulder, N. C. Coops, J. Linke, G. McDermid, J. G. Masek, F. Gao, and J. C. White, "A new data fusion model for high spatial- and temporal-resolution mapping of forest disturbance based on Landsat and MODIS," *Remote Sens. Environ.*, vol. 113, no. 8, pp. 1613–1627, Aug. 2009.
- [9] X. Zhu, J. Chen, F. Gao, X. Chen, and J. G. Masek, "An enhanced spatial and temporal adaptive reflectance fusion model for complex heterogeneous regions," *Remote Sens. Environ.*, vol. 114, no. 11, pp. 2610–2623, Nov. 2010.

- [10] E. F. Vermote, S. Y. Kotchenova, and J. P. Ray. MODIS Surface Reflectance User's Guide v 1.2. [Online]. Available: <http://modis-sr.ltdri.org>
- [11] M. Feng, J. Sexton, C. Huang, J. Masek, E. Vermote, F. Gao, R. Narasimhan, S. Channan, R. Wolfe, and J. Townshend, "Global surface reflectance products from Landsat: Assessment using coincident MODIS observations," *Remote Sens. Environ.*, vol. 134, pp. 276–293, July 2013.
- [12] S. P. Healey, W. B. Cohen, Z. Yang, and O. N. Krankina, "Comparison of tasseled cap-based Landsat data structures for use in forest disturbance detection," *Remote Sens. Environ.*, vol. 97, no. 3, pp. 301–310, Aug. 2005.
- [13] X. Zhang, C. Schaaf, M. A. Friedl, A. Strahler, F. Gao, and J. Hodges, "MODIS tasseled cap transformation and its utility," in *Proc. IEEE Int. Geoscience Remote Sensing Symp.*, 2002, pp. 1063–1065.
- [14] V. Emelyanova, T. R. McVicar, T. G. van Niel, L. T. Li, and A. I. J. M. van Dijk, "Assessing the accuracy of blending Landsat-MODIS surface reflectances in two landscapes with contrasting spatial and temporal dynamics: A framework for algorithm selection," *Remote Sens. Environ.*, vol. 133, no. 15, pp. 193–209, June 2013.
- [15] T. Hilker, M. A. Wulder, N. C. Coops, N. Seitz, J. C. White, F. Gao, J. G. Masek, and G. Stenhouse, "Generation of dense time series synthetic Landsat data through data blending with MODIS using a spatial and temporal adaptive reflectance fusion model," *Remote Sens. Environ.*, vol. 113, no. 9, pp. 1988–1999, Sept. 2009.
- [16] M. Schmidt, T. Udelhoven, T. Gill, and A. Röder, "Long term data fusion for a dense time series analysis with MODIS and Landsat imagery in an Australian Savanna," *J. Appl. Remote Sens.*, vol. 6, no. 1, p. 063512, May 2012.
- [17] D. Singh, "Generation and evaluation of gross primary productivity using Landsat data through blending with MODIS data," *Int. J. Appl. Earth Observ.*, vol. 13, no. 1, pp. 59–69, Feb. 2011.
- [18] J. D. Watts, S. L. Powell, R. L. Lawrence, and T. Hilker, "Improved classification of conservation tillage adoption using high temporal and synthetic satellite imagery," *Remote Sens. Environ.*, vol. 115, no. 1, pp. 66–75, Jan. 2011.
- [19] J. J. Walker, K. M. de Beurs, R. H. Wynne, and F. Gao, "Evaluation of Landsat and MODIS data fusion products for analysis of dryland forest phenology," *Remote Sens. Environ.*, vol. 117, pp. 381–393, Feb. 2012.
- [20] F. Gao, P. Wang, and J. Masek, "Integrating remote sensing data from multiple optical sensors for ecological and crop condition monitoring," in *Proc. SPIE 8869, Remote Sensing Modeling Ecosystems Sustainability X*, 2013.
- [21] Q. Weng, P. Fu, and F. Gao, "Generating daily land surface temperature at Landsat resolution by fusing Landsat and MODIS data," *Remote Sens. Environ.*, vol. 145, no. 5, pp. 55–67, Apr. 2014.
- [22] C. Cammalleri, M. C. Anderson, F. Gao, C. R. Hain, and W. P. Kustas, "A data fusion approach for mapping daily evapotranspiration at field scale," *Water Resources Res.*, vol. 49, no. 8, pp. 4672–4686, Aug. 2013.
- [23] C. Cammalleri, M. C. Anderson, F. Gao, C. R. Hain, and W. P. Kustas, "Mapping daily evapotranspiration at field scales over rainfed and irrigated agricultural areas using remote sensing data fusion," *Agric. Forest Meteorol.*, vol. 186, pp. 1–11, Mar. 2014.
- [24] P. Wang, F. Gao, and J. Masek, "Operational data fusion framework for building frequent Landsat-like images in cloudy regions," *IEEE Trans. Geosci. Remote Sens.*, vol. 52, no. 11, pp. 7,353–7,365, Nov. 2014.
- [25] A. Berland, T. Nelson, G. Stenhouse, K. Graham, and J. Cranton, "The impact of landscape disturbance on grizzly bear habitat use in the foothills model forest, Alberta, Canada," *Forest Ecol. Manage.*, vol. 256, no. 11, pp. 1875–1883, Nov. 2008.
- [26] P. M. Fearnside, "Global warming and tropical land-use change: greenhouse gas emissions from biomass burning, decomposition and soils in forest conversion, shifting cultivation and secondary vegetation," *Climatic Change*, vol. 46, nos. 1–2, pp. 115–158, June 2000.
- [27] R. A. Pielke, G. Marland, R. A. Betts, T. N. Chase, J. L. Eastman, J. O. Niles, D. D. S. Niyogi, and S. W. Running, "The influence of land-use change and landscape dynamics on the climate system: Relevance to climate-change policy beyond the radiative effect of greenhouse gases," *Philos. Trans. A, Math. Phys. Eng. Sci.*, vol. 360, no. 1797, pp. 1705–1719, Aug. 2002.
- [28] M. Hansen, P. V. Potapov, R. Moore, M. Hancher, S. A. Turubanova, A. Tyukavina, D. Thau, S. V. Stehman, S. J. Goetz, T. R. Loveland, A. Kommareddy, A. Egorov, L. Chini, C. O. Justice, and J. R. G. Townshend, "High-resolution global maps of 21st-century forest cover change," *Science*, vol. 342, no. 6160, pp. 850–853, Nov. 2013.
- [29] R. M. Scheller, J. B. Domingo, B. R. Sturtevant, J. S. Williams, A. Rudy, E. J. Gustafson, and D. J. Mladenoff, "Design, development, and application of LANDIS-II, a spatial landscape simulation model with flexible temporal and spatial resolution," *Ecol. Model.*, vol. 201, nos. 3–4, pp. 409–419, Mar. 2007.
- [30] M. C. Hansen, S. V. Stehman, P. V. Potapov, T. R. Loveland, J. R. G. Townshend, R. S. DeFries, K. W. Pittman, B. Arunarwati, F. Stolle, M. K. Steininger, M. Carroll, and C. DiMiceli, "Humid tropical forest clearing from 2000 to 2005 quantified by using multitemporal and multiresolution remotely sensed data," in *Proc. Nat. Academy Sciences United States America*, 2008, vol. 105, no. 27, pp. 9439–9444.
- [31] W. F. Laurance, D. C. Useche, J. Rendeiro, M. Kalka, C. J. A. Bradshaw, S. P. Sloan, et al. "Averting biodiversity collapse in tropical forest protected areas," *Nature*, vol. 489, no. 7415, pp. 290–294, July 2012.
- [32] R. Gaulton, T. Hilker, M. A. Wulder, N. C. Coops, and G. Stenhouse, "Characterizing stand-replacing disturbance in western Alberta grizzly bear habitat, using a satellite-derived high temporal and spatial resolution change sequence," *Forest Ecol. Manage.*, vol. 261, no. 4, pp. 865–877, Feb. 2011.
- [33] C. J. Kucharik, "A multidecadal trend of earlier corn planting in the central USA," *Agron. J.*, vol. 98, no. 6, pp. 1544–1550, Oct. 2006.
- [34] P. Jonsson and L. Eklundh, "TIMESAT—A program for analysing time-series of satellite sensor data," *Comput. Geosci.*, vol. 30, no. 8, pp. 833–845, Oct. 2004.
- [35] D. Kalma, T. R. McVicar, and M. F. McCabe, "Estimating land surface evaporation: A review of methods using remotely sensing surface temperature data," *Survey Geophys.*, vol. 29, nos. 4–5, pp. 421–469, Oct. 2008.
- [36] M. C. Anderson, R. G. Allen, A. Morse, and W. P. Kustas, "Use of Landsat thermal imagery in monitoring evapotranspiration and managing water resources," *Remote Sens. Environ.*, vol. 122, pp. 50–65, July 2012.
- [37] G. Sun, A. Noormets, M. J. Gavazzi, S. G. McNulty, J. Chen, J.-C. Domec, J. S. King, D. M. Amatya, and R. W. Skaggs, "Energy and water balance of two contrasting loblolly pine plantations on the lower coastal plain of North Carolina, USA," *Forest Ecol. Manage.*, vol. 259, no. 7, pp. 1299–1310, Mar. 2010.
- [38] J.-C. Domec, G. Sun, A. Noormets, M. J. Gavazzi, E. A. Treasure, E. Cohen, J. J. Swenson, S. G. McNulty, and J. S. King, "A comparison of three methods to estimate evapotranspiration in two contrasting Loblolly Pine plantations: Age-related changes in water use and drought sensitivity of evapotranspiration components," *Forest Sci.*, vol. 58, no. 5, pp. 497–512, 2012.
- [39] C. B. Schaaf, F. Gao, A. H. Strahler, W. Lucht, X. W. Li, T. Tsang, N. C. Strugnell, X. Y. Zhang, Y. F. Jin, J. P. Muller, P. Lewis, M. Barnsley, P. Hobson, M. Disney, G. Roberts, M. Dunderdale, C. Doll, R. P. d'Entremont, B. X. Hu, S. L. Liang, J. L. Privette, and D. Roy, "First operational BRDF, albedo and nadir reflectance products from MODIS," *Remote Sens. Environ.*, vol. 83, nos. 1–2, pp. 135–148, Nov. 2002.